Journal of Microscopy, Vol. 202, Pt 1, April 2001, pp. 60–65.
Received 28 August 2000; accepted 1 December 2000

Non-regularly shaped plasmon resonant nanoparticle as localized light source for near-field microscopy

J. P. KOTTMANN*, O. J. F. MARTIN*, D. R. SMITH† & S. SCHULTZ†
**Electromagnetic Fields and Microwave Electronics Laboratory, Swiss Federal Institute of Technology, ETH-Zentrum, Gloriastrasse 35, 8092 Zurich, Switzerland*
†Department of Physics, University of California, San Diego, 9500 Gilman Drive, La Jolla, California 92093-0319, U.S.A.

Key words. Local probe microscopy, localized light source, near-field optics, numerical simulations, optics of metal, plasmon-polariton, plasmon resonance, surface enhanced Raman scattering.

Summary

We study numerically two-dimensional nanoparticles with a non-regular shape and demonstrate that these particles can support many more plasmon resonances than a particle with a regular shape (e.g. an ellipse). The electric field distributions associated with these different resonances are investigated in detail in the context of near-field microscopy. Depending on the particle shape, extremely strong and localized near-fields, with intensity larger than 10^5 that of the illumination wave, can be generated. We also discuss the spectral dependence of these near-fields and show that different spatial distributions are observed, depending which plasmon resonance is excited in the particle.

Introduction

A powerful, yet well localized source of light is probably the most important prerequisite for scanning near-field optical microscopy (SNOM). Such a source is in most instances realized by scattering some incident field on a small volume of polarizable matter with permittivity $\varepsilon(\lambda)$ (apertureless probes work exactly with this principle; for an aperture probe, one can consider that the very tip plays the role of polarizable volume).

The scattering efficiency for a polarizable volume with a spherical shape, in vacuum, is given by (Bohren & Huffman, 1983)

$$Q(\lambda) = \frac{8}{3} x^4 \left| \frac{\varepsilon(\lambda) - 1}{\varepsilon(\lambda) + 2} \right|^2, \qquad (1)$$

where $x = 2\pi R/\lambda$ is the size parameter for the sphere, R its radius and λ the wavelength. Equation (1) holds when $R << \lambda$.

Correspondence: Dr O. J. F. Martin. Tel.: +41 1 632 5722; fax: +41 1 632 1647; e-mail: martin@ifh.ee.ethz.ch

From Eq. (1) it is clear that the scattered field, and therefore the corresponding source intensity, for SNOM can be increased by raising the size parameter x (i.e. the sphere radius R). This, however, is not favourable for SNOM because a larger source impinges on the resolution.

Another possibility to increase the source intensity is to augment the dielectric contrast $\varepsilon(\lambda) - 1$. Unfortunately, quite important variations of the permittivity are required to increase $Q(\lambda)$ in a noticeable manner. Furthermore, large permittivity materials at optical frequencies (like semiconductors) have a strong absorption, so that most of the field would be absorbed in the sphere.

The most effective way to realize a strong localized source with such a sphere is therefore to play with the denominator in Eq. (1). As a matter of fact, when $\varepsilon = -2$, the scattered field explodes. This corresponds to the excitation of a so-called plasmon resonance in the particle (Ruppin, 1982). At optical frequencies, this condition can be fulfilled for different metals. In the present work we shall concentrate on silver, using the experimental data of Johnson & Christy (1972) for $\varepsilon(\lambda)$.

Plasmon resonances and the extremely large electromagnetic fields associated with them are playing a key role in surface-enhanced Raman scattering (Metiu, 1984; Moskovits, 1985). In near-field optics they have been used in subtle tip configurations for imaging (Koglin *et al.*, 1995) or Raman spectroscopy (Stöckle *et al.*, 2000) and their optical response has been investigated experimentally using photon scanning tunnelling microscope (Hecht *et al.*, 1996; Krenn *et al.*, 1999a, b; Weeber *et al.*, 1999)

However, very little is known about the relationship between the spectrum of plasmon resonances and the particle shape. Equation (1) shows that a small sphere has one single resonance, occurring at the wavelength λ_{res} where $\varepsilon(\lambda_{res}) \cong -2$. A spheroid has two plasmon resonances,

associated with its two principal axes (Bohren & Huffman, 1983), but no theory exists for nanoparticles with an arbitrary shape (except maybe Fuchs, 1975, who studied the response of a small cube in the electrostatic approximation). This is quite surprising because one can expect that the particle shape is determinant for the number and strength of resonances that can be excited in the particle. Actually this fact was already noticed in the middle of the 19th century by Faraday, who realized that gold colloids were giving their strong colours to stained glass and wrote: 'that a mere variation in the size of its particles gave rise to a variety of colours' (Kerker, 1991).

Very recently, we demonstrated that nanowires (i.e. two-dimensional (2D) nanoparticles) had indeed a very complex resonances spectrum that strongly depended on the particle shape (Kottmann *et al.*, 2000b, c).

The objective of the present publication is to study the implications of this complex spectrum of plasmon resonances for near-field optical microscopy. In particular, we will investigate the localization of the electromagnetic field associated with these different resonances.

The numerical results presented in this paper were obtained using a newly developed finite elements techniques for scattering calculations. This technique is described in detail in Kottmann & Martin (2000), where its convergence and accuracy for the computation of plasmon resonant nanoparticles is also assessed. The particles are typically discretized with 3000 triangular elements. In the following we will consider particles with sharp corners, which introduces additional numerical difficulties, as the field becomes singular at short distance from an infinitely sharp, perfectly conducting corner. However, the sharpness of a real particle is limited by surface and boundary energies; therefore, we have rounded off each corner by 0.25 nm, providing a more realistic model and removing the numerical instabilities.

Results

Spectral response

Before investigating complex shape particles, it is educative to start with a regular geometry. Figure 1 gives the scattering cross-section (SCS) for an elliptical particle (SCS have nm units because we are dealing with 2D particles). Depending on the illumination direction, two different resonances can be excited in this geometry: each resonance being associated with one principle axis. For incidence in a direction off either of the principal axes, both resonances are excited (Fig. 1).

If now we consider a particle with a lower symmetry, we obtain a much more complex response, as illustrated in Fig. 2 for two triangular particles with the same area. For the equilateral particle three plasmon resonances are visible. This number increases further for the right-angled

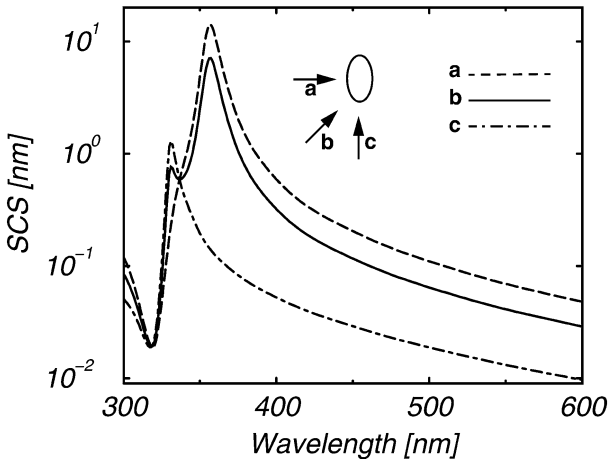

Fig. 1. Scattering cross-section (SCS) for a 10×20 nm^2 elliptical particle, for three different illumination directions a, b and c.

triangle. These resonances now cover a much broader wavelength range, up to $\lambda = 500$ nm for the first resonance of the right angled particle (the first resonance is that corresponding to the lowest energy, i.e. the longest wavelength). In Fig. 2 the very large SCS associated with this resonance is striking, five times larger than for the first resonance of the equilateral triangle, although both particles have the same area.

As for the elliptical particle, it is important to keep in mind that the SCS depends on the illumination direction. This dependence is actually stronger when the symmetry of the particle is reduced. The SCS reported in Fig. 2, as well as the different results presented in the next section, were obtained with particle illumination from the left (i.e. corresponding to the illumination direction a in Fig. 1).

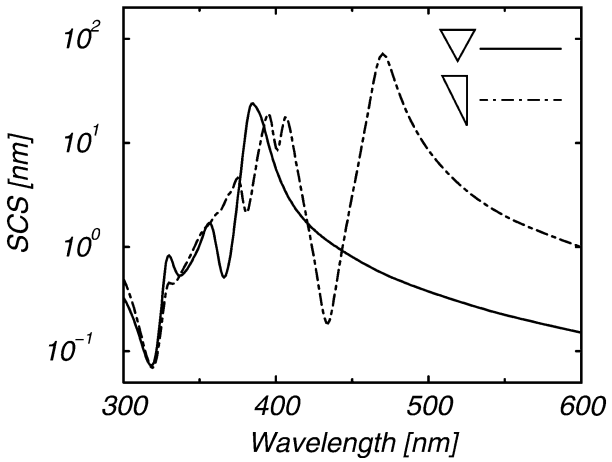

Fig. 2. Scattering cross-section (SCS) for an equilateral triangle (side 27 nm) and a right-angled triangle with the same area and a 1 : 2 base : perpendicular ratio (base 17.8 nm). The particle is illuminated from the left side, corresponding to direction a in Fig. 1.

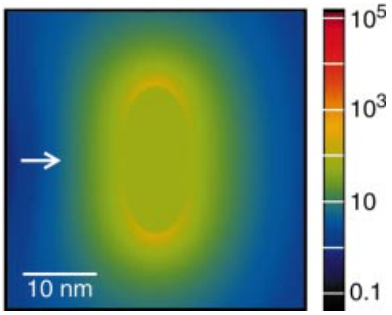

Fig. 3. Relative electric field intensity distribution for the elliptical particle described in Fig. 1, at the main resonance ($\lambda = 359$ nm). The arrow indicates the illumination direction.

Near-field enhancement

For SNOM applications, it is not the field scattered far away which is relevant, but the near-field in close vicinity of the particle. We shall therefore now concentrate on the near-field distribution generated by the particles discussed in the previous section.

Again we start with the simple elliptical particle. The electric field intensity distribution at the main resonance is reported in Fig. 3. For all the calculations presented in this section the intensity of the incident plane wave is one, the logarithmic colour scale in Fig. 3 gives directly, therefore, the intensity enhancement generated by the small metallic particle. To ease comparison, we will use the same colour scale throughout the paper.

The field intensity at the particle apex reaches about 200 times the incident intensity. This plasmon resonance is associated with polarization charges of a given sign accumulating at one end of the particle while opposite charges accumulate at the other end. During one period these polarization charges oscillate between the two extremities, as illustrated in the movies presented in (Kottmann *et al.*, 2000a). The field inside the particle remains quite homogeneous.

This is not at all the case for the equilateral triangle, as illustrated in Fig. 4. At the main resonance the field intensity reaches 3×10^4 that of the incident field. This dramatic enhancement is caused by polarization charges accumulating at the particle tip, while opposite charges are distributed on the adjacent sides (Kottmann *et al.*, 2000a). The fact that all corners light up is related to the particular illumination direction. If the particle was illuminated along one of its symmetry axes, only the two corners transverse to the illumination direction would light up.

The second resonance [$\lambda = 358$ nm, Fig. 4(b)], produces a somewhat reduced intensity enhancement, in the order of 3.5×10^3. The field distribution at the vicinity of the tip is also different, with two side lobes and a lower field intensity in the forward direction (Fig. 4(b)). In this mode plus and minus polarization charges accumulate in the corner, which produces this field distribution pattern (Kottmann *et al.*, 2000a).

It is extremely important to realize that these plasmon resonances are no lightning rod or tip effects, but truly resonances related to the overall particle shape. The lightning rod effect, occurring when the particle is off-resonance, provides a much weaker intensity enhancement, reaching, for example, 70 at $\lambda = 600$ nm, although the permittivity of silver is quite high at this wavelength: $\varepsilon = (-16 + i0.4)$ (Fig. 4(d)).

The small resonance at $\lambda = 329$ nm (Fig. 4(a)) is quite interesting: it exists for any non-regularly shaped particle, independent of the illumination direction (see Fig. 2). It corresponds to the bulk plasmons and occurs at the wavelength λ_{bulk} where $\varepsilon(\lambda_{bulk}) \cong 0$ (Ruppin, 1982). Contrary to the surface plasmon previously investigated, the bulk plasmon is a longitudinal mode. This explains why only the two edges in the propagation direction and not the particle apex light up in Fig. 4(a).

This bulk mode is also visible for the right-angled particle (Fig. 5(a); see also the SCS in Fig. 2). The intensity enhancement associated with the main plasmon resonance of this particle reaches 7×10^5, with a field distribution similar to a point source (Fig. 5(d)). Higher order

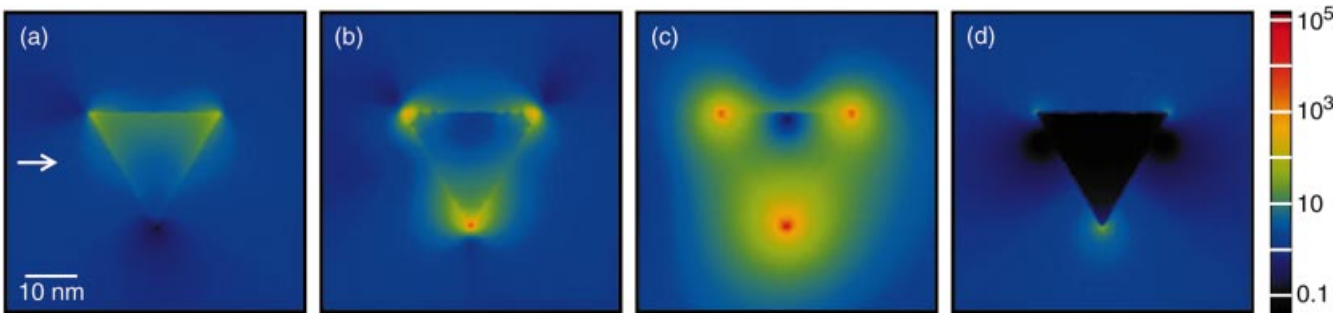

Fig. 4. Relative electric field intensity distribution for a 27 nm equilateral triangle for three different plasmon resonances: (a) $\lambda = 329$ nm, (b) $\lambda = 358$ nm and (c) $\lambda = 385$ nm (compare the wavelength with the SCS given in Fig. 2). (d) Out of resonance, at $\lambda = 600$ nm. The arrow indicates the illumination direction for all figures.

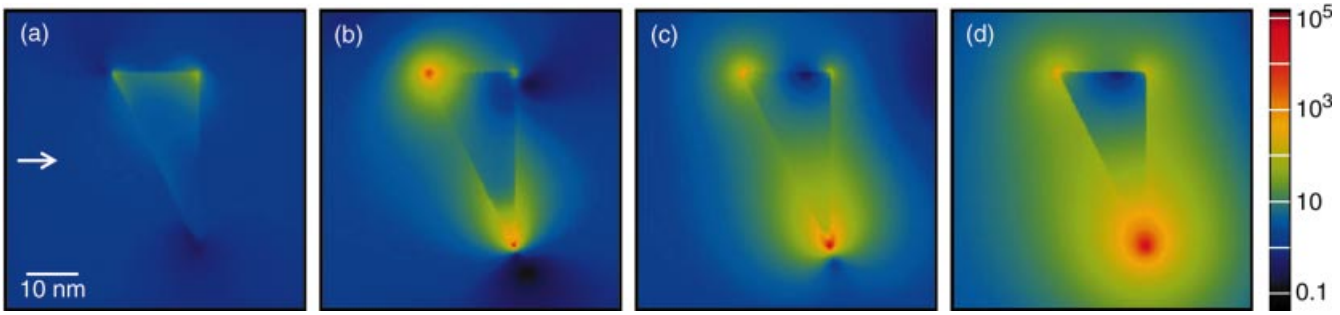

Fig. 5. Relative electric field intensity distribution for a right-angled triangle of same area as that in Fig. 4 and with a 1 : 2 base : perpendicular ratio. Four different plasmon resonances are investigated: (a) $\lambda = 329$ nm, (b) $\lambda = 375$ nm, (c) $\lambda = 406$ nm and (d) $\lambda = 470$ nm (compare the wavelength with the SCS given in Fig. 2). The arrow indicates the illumination direction for all figures.

resonances also generate quite a strong field enhancement, with a more complex field distribution (Fig. 5(b) and (c)). Again, this behaviour can be related to the polarization charges that accumulate on the particle surface (Kottmann *et al.*, 2000a).

The previous figures illustrated the extremely intense electromagnetic field that can be produced by non-regularly shaped plasmon resonant particles. As mentioned in the Introduction, it is mandatory for high resolution SNOM applications that these fields are also strongly localized. To quantify this localization let us now investigate the variation of the field distribution at the immediate vicinity of the particle.

In Fig. 6 we report the relative field intensity when one moves away from the particle tip, for three different particle shapes at their main resonance. First, note that the field intensity at the surface of the particle is about 10 000 times stronger for the right-angled triangle than for the elliptical particle. Furthermore, the field is much more localized for the non-regularly shaped particles: over the first nanometre the intensity decreases by a factor of about 120, respectively 24, for the right-angled, respectively equilateral triangle; whereas it decreases only by a factor of three for the elliptical particle.

For a non-regular particle with several resonances, the near-field intensity distribution depends on the mode excited in the particle, as illustrated in Fig. 7. In this figure we observe that the field decays more rapidly for the second resonance ($\lambda = 358$ nm) than for the first one ($\lambda = 385$ nm). This behaviour can be related to the charge distribution associated with each resonance. Indeed, as illustrated in Kottmann *et al.* (2000a) and mentioned in the discussion of Figs 3 and 4, the main resonance is associated with polarization charges of similar sign accumulating at

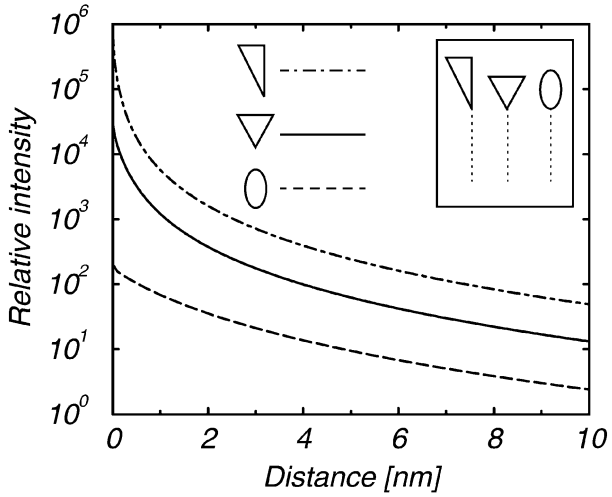

Fig. 6. Relative electric field intensity as a function of the distance from the particle corner (dotted line in the inset), for three different particle shapes at their main resonance (ellipse: $\lambda = 359$ nm, equilateral triangle: $\lambda = 385$ nm, right-angled triangle: $\lambda = 470$ nm).

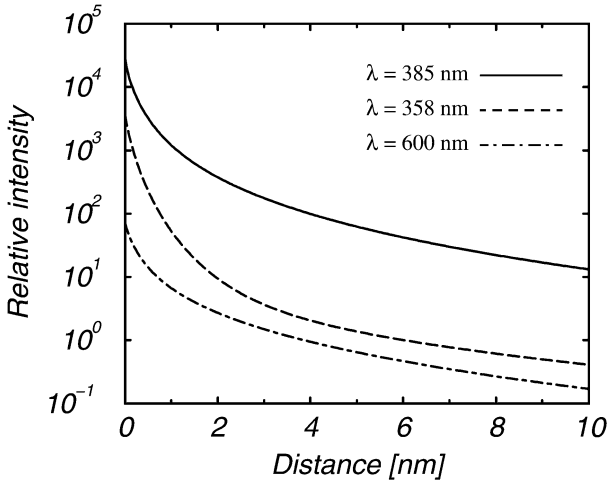

Fig. 7. Relative electric field intensity for the equilateral triangle as a function of the distance from the particle corner (dotted line in the inset in Fig. 6). The field intensity is computed for two plasmon resonances ($\lambda = 385$ nm and $\lambda = 358$ nm) and out of resonance at $\lambda = 600$ nm.

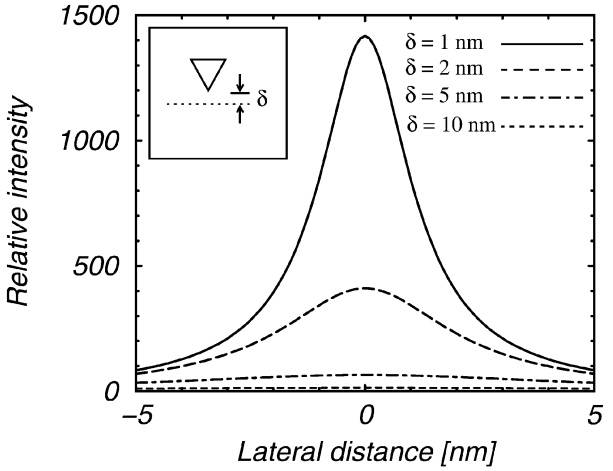

Fig. 8. Lateral relative electric field intensity distribution, at different distances δ from the equilateral triangle tip, at the main resonance ($\lambda = 385$ nm).

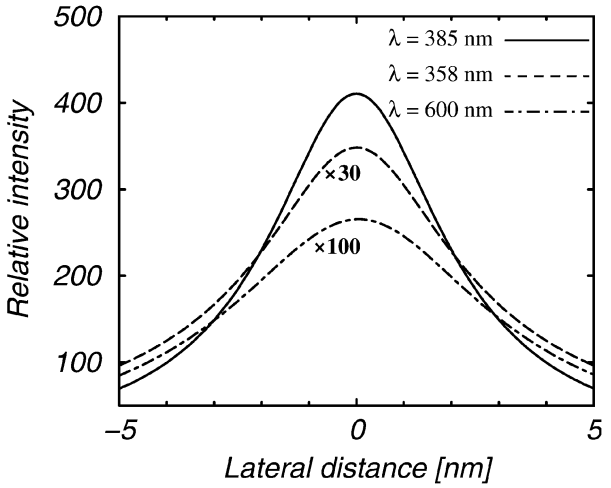

Fig. 9. Lateral relative electric field intensity distribution at a $\delta = 2$ nm distance from the equilateral triangle tip, for two plasmon resonances ($\lambda = 385$ nm and $\lambda = 358$ nm) and out of resonance at $\lambda = 600$ nm.

the particle corner, whereas higher order resonances have a more complex polarization charge distribution with plus and minus charges accumulating at the corner. The former charge distribution produces therefore a near-field intensity distribution similar to that of a point source (i.e. $\sim 1/d^2$, where d is the distance), whereas the latter produces a near-field intensity distribution similar to that of a dipole (i.e. $\sim 1/d^6$). This explains the distance dependences observed in Fig. 7. This difference of behaviour as a function of the resonance, i.e. of the illumination wavelength, could be evidenced in experimental SNOM approach curves.

At distances larger than say 5 nm, the decay of the field intensity as a function of the distance is similar for the different resonances (Fig. 7). The field generated by the main resonance remains about 50 times stronger than that of the other resonance. Choosing the correct illumination wavelength can therefore have a dramatic influence on the light throughput in a SNOM experiment, even for constant height scans at some distances from the sample under study.

The extremely important dynamic range also observed for the right-angled particle in Fig. 7 could be useful in an apertureless SNOM experiment, where the tip is vibrated vertically above the sample.

The other deciding factor that determines the resolution in a SNOM experiment is the lateral field confinement. In Fig. 8 we report the lateral field distribution in the main resonance, at different distances δ from the tip of the equilateral particle. Striking is the strong lateral confinement, with a 2.5 nm full width half-maximum (FWHM) for $\delta = 1$ nm. This lateral confinement decreases for larger distances: for $\delta = 2$ nm we obtain FWHM = 4.5 nm and for $\delta = 5$ nm, FWHM = 10 nm. However, it is important to note that the field at close vicinity of the particle is confined on dimensions much smaller than the particle size (27 nm in that case).

As expected, the lateral field confinement also depends on the plasmon resonance that is excited, as illustrated in Fig. 9. Although the corresponding peak intensity is much weaker, it is interesting to note in this figure that the field obtained out of resonance is also well confined (FWHM for the first plasmon resonance: 4.5 nm, for the second resonance: 5.8 nm and out of resonance: 6.8 nm).

Finally we compare in Fig. 10 the lateral confinement for the three different particle shapes. As already discussed, the right-angled triangle produces by far the strongest field. Its

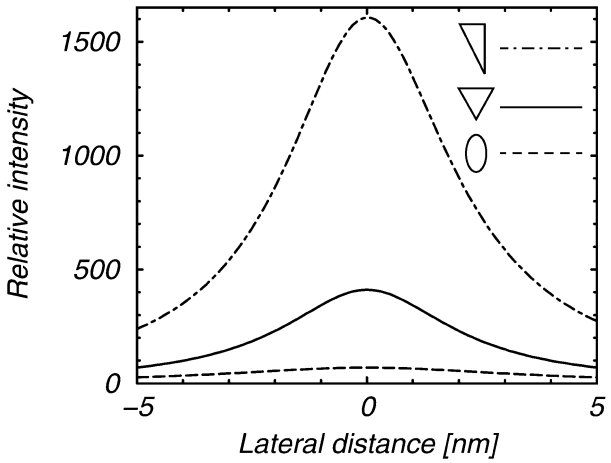

Fig. 10. Lateral relative electric field intensity distribution at a $\delta = 2$ nm distance from the particle surface, for three different particle shapes at their main resonance (ellipse: $\lambda = 359$ nm, equilateral triangle: $\lambda = 385$ nm, right-angled triangle: $\lambda = 470$ nm).

lateral confinement (FWHM = 4.4 nm) is similar to that of the equilateral triangle. By contrast, the elliptical particle has a lateral confinement only in the order of the particle size (FWHM = 8 nm).

Conclusion

We have demonstrated that two-dimensional particles in the 20–50 nm range with a non-regular section, for example a triangular section, have a much more complex spectrum of plasmon resonances than a regularly shaped particle, like an ellipse. Furthermore, the plasmon resonances for non-regular particles extend over a broader part of the wavelength spectrum.

These resonances are associated with extremely strong near-fields, with intensities larger than 10^5 that of the illumination wave. The implications of these strong near-fields for optical microscopy, as well as their spatial and spectral behaviour, have been discussed in detail.

These new theoretical insights increase our understanding of plasmon resonances in non-regularly shaped particles and should pave the way towards the utilization of specific particle shapes to boost the resolution, light throughput and spectral sensitivity of near-field microscopy.

Acknowledgements

This work was supported by the Swiss National Science Foundation and by the U.S. NSF (NSF-DMR-96-23949 and NSF-DMR-97-24535).

References

Bohren, C.F. & Huffman, D.R. (1983) *Absorption and Scattering of Light by Small Particles*. Wiley, New York.

Fuchs, R. (1975) Theory of the optical properties of ionic crystal cubes. *Phys. Rev. B*, **11–4**, 1732–1740.

Hecht, B., Bielfeldt, H., Novotny, L., Inouye, Y. & Pohl, D.W. (1996) Local excitation, scattering, and interference of surface plasmons. *Phys. Rev. Lett*. **77–9**, 1889–1892.

Johnson, P.B. & Christy, R.W. (1972) Optical constants of the noble metals. *Phys. Rev. B*, **6–12**, 4370–4379.

Kerker, M. (1991) Founding fathers of light scattering and surface-enhanced Raman scattering. *Appl. Optics*, **30–33**, 4699–4705.

Koglin, J., Fischer, U.C., Brzoska, K.D., Göhde, W. & Fuchs, H. (1995) The tetrahedral tip as a probe for scanning near-field optical and for scanning tunneling microscopy. *Photons and Local Probes* (ed. by O. Marti and R. Möller), pp. 79–92. NATO ASI Series, Deel 300. Kluwer, Dordrecht.

Kottmann, J.P. & Martin, O.J.F. (2000) Accurate solution of the volume integral equation for high permittivity scatterers. *IEEE Trans. Antennas Propag.* **48**, in press.

Kottmann, J.P., Martin, O.J.F., Smith, D.R. & Schultz, S. (2000a) Field polarization and polarization charge distributions in plasmon resonant particles. *New J. Phys*. **2**, 21.1–27.9.

Kottmann, J.P., Martin, O.J.F., Smith, D.R. & Schultz, S. (2000b) Spectral response of silver nanoparticles. *Optics Express*, **6–11**, 213–219.

Kottmann, J.P., Martin, O.J.F., Smith, D.R. & Schultz, S. (2000c) Dramatic localized electromagnetic enhancement in plasmon resonant nanowires. *Chem. Phys. Lett.* in press.

Krenn, J.R., Dereux, A., Weeber, J.C., Bourillot, E., Lacroute, Y., Goudonnet, J.P., Schider, G., Gotschy, W., Leitner, A., Aussenegg, en, F.R. & Girard, C. (1999a) Squeezing the optical near-field by plasmon coupling of metallic nanoparticles. *Phys. Rev. Lett*. **82**, 2590–2593.

Krenn, J.R., Weeber, J.C., Bourillot, E., Dereux, A., Goudonnet, J.P., Schider, G., Leitner, A., Aussenegg, F.R. & Girard, C. (1999b) Direct observation of localized surface plasmons coupling. *Phys. Rev. B*, **60**, 5029–5033.

Metiu, H. (1984) Surface enhanced spectroscopy. *Prog. Surf. Sci*. **17**, 153–320.

Moskovits, M. (1985) Surface-enhanced spectroscopy. *Rev. Mod. Phys*. **57**, 783–826.

Ruppin, R. (1982) Spherical and cylindrical surface polaritons in solids. *Electromagnetic Surface Modes* (ed. by A. D. Boardman), pp. 345–398. Wiley, Chichester.

Stöckle, R.M., Suh, Y.D., Deckert, V. & Zenobi, R. (2000) Nanoscale chemical analysis by tip-enhanced Raman spectroscopy. *Chem. Phys. Lett*. **318**, 131–136.

Weeber, J.-C., Dereux, A., Girard, C., Krenn, J.R. & Goudonnet, September, J.-P. (1999) Plasmon polaritons of metallic nanowires for controlling submicron propagation of light. *Phys. Rev. B*, **60–12**, 9061–9068.